Unravelling the ultrastructure of stress granules and associated P-bodies in human cells

Sylvie Souquere*, Stéphanie Mollet*, Michel Kress, François Dautry, Gérard Pierron‡ and Dominique Weil‡

CNRS FRE2937, Institut André Lwoff, 94800 Villejuif, France

*These authors contributed equally to this work

‡Authors for correspondence (weil@vjf.cnrs.fr; pierron@vjf.cnrs.fr)

Accepted 1 August 2009

Journal of Cell Science 122, 3619-3626 Published by The Company of Biologists 2009

doi:10.1242/jcs.054437

Summary

Stress granules are cytoplasmic ribonucleoprotein granules formed following various stresses that inhibit translation. They are thought to help protecting untranslated mRNAs until stress relief. Stress granules are frequently seen adjacent to P-bodies, which are involved in mRNA degradation and storage. We have previously shown in live cells that stress granule assembly often takes place in the vicinity of pre-existing P-bodies, suggesting that these two compartments are structurally related. Here we provide the first ultrastructural characterization of stress granules in eukaryotic cells by electron microscopy. Stress granules resulting from oxidative stress, heat-shock or protein overexpression are loosely organised fibrillo-granular aggregates of a moderate electron density, whereas P-bodies are denser and fibrillar. By in situ hybridization at the electron microscopic level, we show that stress granules are enriched in poly(A)$^+$ mRNAs, although these represent a minor fraction of the cellular mRNAs. Finally, we show that, despite close contact with P-bodies, both domains remain structurally distinct and do not interdigitate.

Supplementary material available online at
http://jcs.biologists.org/cgi/content/full/122/20/3619/DC1

Key words: Stress response, mRNA storage, mRNA degradation

Introduction

The function of coding mRNAs is controlled by their translation rate as well as by storage and degradation. Stress granules and P-bodies are two structures recently shown to concentrate untranslated mRNAs in the cytoplasm of mammalian cells, and are thought to participate in mRNA storage and degradation (Eulalio et al., 2007). Stress granules appear only during stresses that massively repress translation, such as oxidative stress, heat shock and UV irradiation (Anderson and Kedersha, 2008), or following the expression of translational regulators such as TIA1 and CPEB1 (Gilks et al., 2004; Wilczynska et al., 2005). They are also induced by viruses that repress the translation of host mRNAs in order to divert the translation machinery toward viral mRNAs (Mazroui et al., 2006; McInerney et al., 2005). Stress granules contain translation initiation factors, proteins of the small but not the large ribosomal subunit, and a large variety of RNA binding proteins. These features suggest a role in the metabolism of arrested mRNAs. Similar granules have recently been observed in yeast following glucose deprivation, which leads to a severe translation inhibition (Hoyle et al., 2007). Stress granules were originally proposed to play a role in the storage of mRNA during stress. However, such a role is difficult to reconcile with dynamic data: in mammals, fluorescence recovery after photobleaching (FRAP) experiments showed that messenger ribonucleoproteins (mRNPs) reside briefly in stress granules (Mollet et al., 2008), and in yeast, translational blockage occurs before stress granule appearance (Buchan et al., 2008). Stress granules could therefore be involved in mRNP remodelling rather than storage.

By contrast, P-bodies contain all proteins known to be involved in the 5′-to-3′ degradation pathway, including the decapping enzyme Dcp2 and its cofactors, and the exonuclease Xrn1. They also contain proteins involved in specific processes leading to mRNA degradation, such as nonsense-mediated decay (NMD) and RNA interference. Mammalian P-bodies are constitutively present in the cells, although their number and size increase with the amount of mRNA to degrade (Cougot et al., 2004; Wilczynska et al., 2005), suggesting that they are active sites of mRNA degradation. More extensive arguments for such a role have been obtained in yeast (Teixeira et al., 2005). In addition to their link to the degradation pathway, P-bodies also participate in the storage of mRNA when its translation is arrested during glucose starvation (Brengues et al., 2005). Similarly, mammalian P-bodies can store mRNAs repressed by miRNA (Bhattacharyya et al., 2006).

In mammals, stress granules and P-bodies contain a few proteins in common, in particular translational repressors such as CPEB1, RAP55 and YB-1 (Wilczynska et al., 2005; Yang and Bloch, 2007; Yang et al., 2006). In addition, stress granules induced in cells previously depleted of P-bodies recruit P-body-specific proteins, such as Dcp1, GW182 and Ge1 (Mollet et al., 2008; Serman et al., 2007). A similar recruitment occurs when stress granules are induced by overexpression of CPEB1 (Wilczynska et al., 2005). This suggests some functional overlap between the two granules. Furthermore, stress granules and P-bodies are frequently seen adjacent to one another, raising the possibility that mRNA and proteins traffic from one to the other structure, thus enabling the two structures to act in concert (Kedersha et al., 2005; Wilczynska et al., 2005). This juxtaposition is the result of some stress granules forming at the contact of pre-existing P-bodies, though further contacts can also be established after stress granule assembly (Kedersha et al., 2005; Mollet et al., 2008). Similar observations have recently been made in yeast, where stress granules not only assemble on P-bodies, but also require P-bodies to assemble (Buchan et al., 2008). Taken together, data obtained in both mammals and yeast raise the question of whether stress granules are structurally related to P-bodies.

Although P-bodies have already been characterized by electron microscopy (Yang et al., 2004), previous descriptions of stress

granules remain elusive. We determined their ultrastructure following various stresses, including oxidative stress, heat shock and protein overexpression. We assessed their identity by immunogold staining and demonstrated enrichment of 18S and depletion of 28S ribosomal RNA by in situ hybridization. Stress granules are less compact than P-bodies, in agreement with their active remodelling behaviour in live cells. Their ultrastructure is granular, and clearly distinct from that of P-bodies, which is more fibrillar. Intimate contacts between the two structures, but not intermingling, were confirmed at high resolution.

Results

Ultrastructure of arsenite-induced stress granules

To study the ultrastructure of cytoplasmic stress granules, HeLa and HEK293 cells were submitted to an oxidative stress (0.5 mM sodium arsenite for 30 minutes). Formation of stress granules was ascertained by immunofluorescence. In parallel, cells were fixed in glutaraldehyde, embedded in Epon, and ultrathin sections of control and treated cells were compared by electron microscopy. As control HeLa and HEK293 cells were indistinguishable, only HeLa cells are shown in Fig. 1A. Following arsenite treatment, all HeLa cells and most of the HEK293 cells contained stress granules as revealed by immunostaining of the stress granule marker eIF3 (Fig. 1B,C, left panels). Electron microscopic observations of lead-citrate-and uranyl-acetate-stained thin sections of the arsenite-treated cells revealed cytoplasmic fibrillo-granular aggregates not seen in control cells (Fig. 1B,C, middle-panels, black arrow). Of a moderate electron density, these spheroid or ellipsoid structures had typical dimensions of 1-2 μm and were present in only about 10% of cell profiles, due to 70 nm thin-sectioning. They were not delineated by a membrane and usually distant from cytoplasmic organelles such as mitochondria or the ER. They were also not found close to the nuclear envelope or of the plasma membrane. By their size, their distribution and their frequency, these aggregates were comparable to the stress granules detected by immunofluorescence. To strengthen this assumption, HeLa cells treated with arsenite as above were washed and further grown in standard medium. As monitored by immunofluorescent staining of TIA1, after 3 hours stress granules disappeared in most cells (not shown). Similarly, ultrastructural observations revealed the disappearance of the cytoplasmic aggregates at this time point (not shown).

To correlate directly ultrastructural observations with immunofluorescence data, we attempted to detect by immunoelectron microscopy the endogenous proteins commonly used as markers of stress granules. Unfortunately, available anti-eIF3 and anti-TIA1 antibodies were ineffective on thin sections of cells embedded in Lowicryl K4M. Therefore, we transfected a TIA1-GFP construct in HEK293 cells which, after 48 hours, were further treated for 30 minutes with arsenite to induce stress granules. Cells were then fixed in glutaraldehyde and embedded in Lowicryl K4M to study the localization of TIA1-GFP using an anti-GFP antibody coupled to 10 nm gold particles. In most transfected cells, the labelling was scarce (3.2±1.1 gold particles per μm^2, n=10) in the cytoplasm and enriched (39±20 gold particles per μm^2, n=10) in cytoplasmic aggregates that were indistinguishable from the arsenite-induced structures seen in Fig. 1B,C (Fig. 2). This accumulation of TIA1-GFP, confirmed the identification of these structures as stress granules. Occasionally, we also detected cells highly labelled with anti-GFP antibodies and containing larger and less uniform cytoplasmic aggregates, which could be induced by TIA1 overexpression independently of arsenite treatment, as shown below.

Ultrastructure of stress granules induced by various agents

To characterize the ultrastructure of stress granules formed in response to different inducers, we first submitted untransfected HeLa cells to heat shock at 42°C for 30 minutes. Stress granule formation

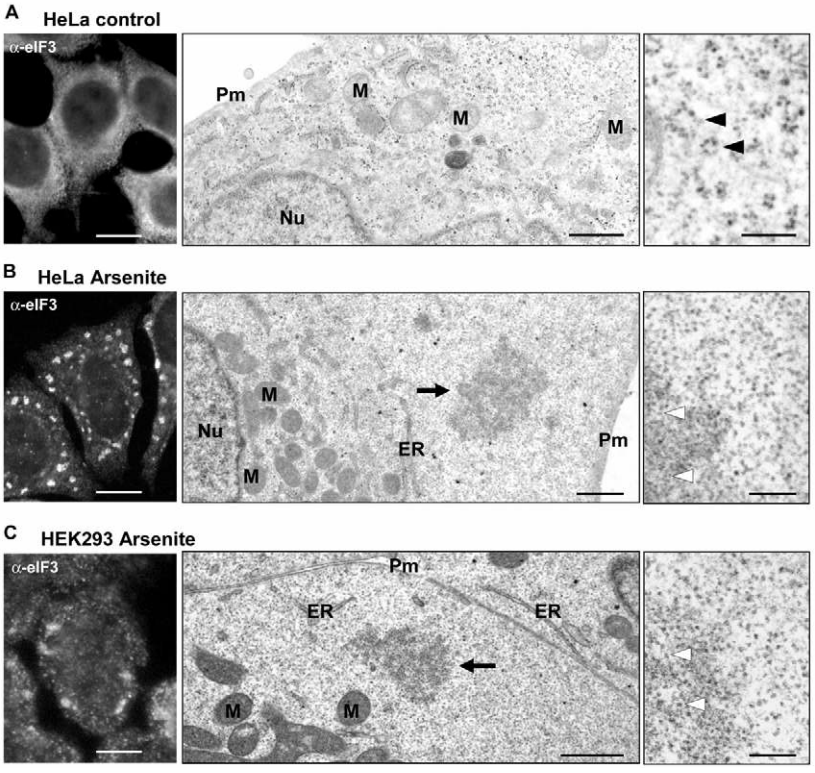

Fig. 1. Ultrastructure of arsenite-induced stress granules in human cells. HeLa (A,B) and HEK293 (C) cells were treated (B,C) or not (A) with arsenite for 30 minutes, as indicated. Cells were then processed for immunofluorescence with anti-eIF3 antibody (left panels) or for electron microscopy (middle panels). Electron microscopic images of glutaraldehyde-fixed, Epon-embedded cells, stained with lead citrate and uranyl acetate are shown. Cytoplasmic granular zones present only in stressed cells are indicated by a black arrow. Pm, plasma membrane; M, mitochondrion; Nu, nucleus. A region including a stress granule and the neighbouring cytosplasm is enlarged in the right panel of B and C, and a region of cytoplasm at the same magnification is shown in the right panel of A. Black arrowheads point to polyribosomes present in the HeLa control cells. The fine granular structure of the cytoplasmic granules in arsenite-treated cells is indicated by white arrowheads. Scale bars: 10 μm, 1 μm and 200 nm for left, middle and right panels, respectively.

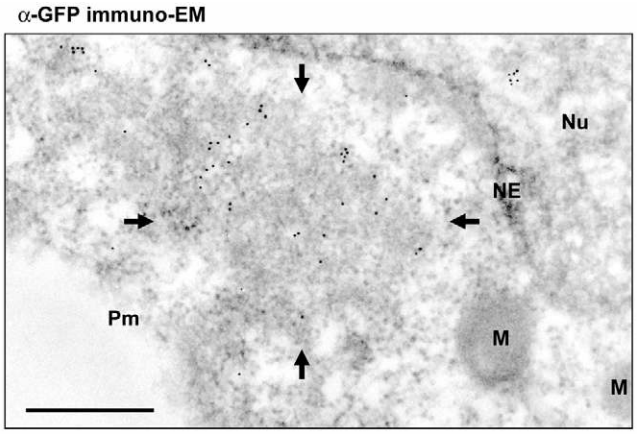

Fig. 2. Accumulation of TIA1-GFP in arsenite-induced stress granules in HEK293 cells. HEK293 cells transfected with TIA1-GFP were treated with arsenite, fixed in glutaraldehyde and embedded in Lowicryl K4M. Thin sections were reacted with a primary anti-GFP antibody and a secondary antibody coupled to 10 nm gold particles. Gold particles are concentrated over a cytoplasmic granule (black arrows) whereas the surrounding cytoplasm, including mitochondria, is weakly labelled. Pm, plasma membrane; NE, nuclear envelope; M, mitochondrion; Nu, nucleus. Uranyl acetate staining. Scale bar: 500 nm.

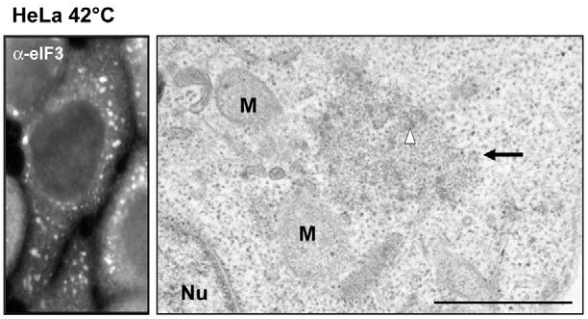

Fig. 3. Ultrastructure of heat shock-induced stress granules in HeLa cells. HeLa cells were incubated at 42°C for 30 minutes and processed for immunofluorescence with anti-eIF3 antibody (left panel) or for electron microscopy (right panel). A heat shock-induced stress granule (black arrow) closely apposed to mitochondria (M) is shown. Note dense fibrillar patches (white arrowhead) within the stress granule. Scale bar: 1 μm.

was monitored by immunofluorescence staining of eIF3 whereas ultrastructural studies were carried out following glutaraldehyde fixation and Epon embedding. As shown in Fig. 3, heat-shock-induced stress granules resembled arsenite-induced stress granules in shape, size and electron density. However, they contained additional dense fibrillar patches (Fig. 3, white arrowheads), and were often closely associated with cytoplasmic organelles such as mitochondria.

TIA1 is one of the proteins that when overexpressed induces stress granules in the absence of further stress, though only in a fraction of the cells (not shown). We therefore examined cells transfected by the TIA1-GFP construct for 48 hours without other treatment. Large and patchy 'stress-granule-like' structures were occasionally observed in the cytoplasm. Following Epon embedding (Fig. 4A), these TIA1-induced granules were seen to have a distinct heterogeneous structure, conferred by electron-dense fibrillar patches interspersed with the granular component. They were also frequently bigger than arsenite- or heat shock-induced stress granules, up to 3-4 μm in size. In Lowicryl-embedded cells, both the nucleus and the cytoplasm were labelled. The occurrence of cytoplasmic granules was restricted to cells containing high levels of cytoplasmic TIA1-GFP (33.5±18 gold particles per μm^2, n=8), and these granules were highly labelled by the anti-GFP antibody (256±110 gold particles per μm^2, n=8; Fig. 4B). It is noteworthy that the TIA1-GFP fusion protein decorated the fibrillar patches that were conspicuous in the TIA1-GFP-dependent stress granules. Similar results were obtained when stress granules were induced by CPEB1-GFP expression (not shown).

Finally, portions of the surrounding cytoplasm were occasionally visible inside the stress granules. This was particularly clear in the TIA1-induced stress granules (Fig. 4A,B), although it could also be observed in stress granules induced by other stresses (Fig. 3). This is consistent with the behaviour of the stress granules seen in live cells, which continuously rearrange with time, with pieces of granules detaching and joining a neighbouring granule, as illustrated in Fig. 4C.

Stress granules formation and translational activity

Electron microscopy made it possible to relate stress granule formation and translational activity on a cell-by-cell basis. Indeed, the conventional organization of the ribosomes in polysomal rosettes (Warner et al., 1962) as observed in control HeLa cells (Fig. 1A, right panel), was lost in all arsenite-treated cells (Fig. 1B,C, right panels), as well as in all heat-shocked cells (Fig. 3). This is consistent with the block in protein synthesis induced by these stresses. Similarly, although polysomal disruption occurs in less than one-third of the TIA1-GFP-transfected cells, the formation of TIA1-induced stress granules was always (n=12) associated with disorganized polysomes (Fig. 4A; supplementary material Fig. S1). The same observations were made for cells containing CPEB1-induced stress granules (not shown), indicating that stress granules are formed only in cells in which translation is severely disturbed. In these conditions, the cytosol was filled with abundant monosomes, with a typical size of 27±4 nm in arsenite-treated cells (n=88). Accordingly, arsenite leads mainly to the accumulation of 80S monosomes, as analysed in sucrose gradients (supplementary material Fig. S2) (Kedersha et al., 2002). The granular component of the stress granules (white arrowheads in Fig. 1B,C, right panels) was the same size (28±4 nm; n=74), suggesting at first sight that monosomes are trapped within the stress granules.

However, stress granules have been shown, using fluorescence microscopy, to be enriched in poly(A)$^+$ mRNA and proteins of the small, but not the large, ribosomal subunit (Kedersha et al., 2002). From these data, it has been speculated that stress granules contain mRNPs assembled into stalled 48S initiation complexes. In order to extend these results, we analysed quantitatively by high resolution in situ hybridization the level of the 18 and 28S ribosomal RNA (rRNA) and of poly(A)$^+$ mRNA in stress granules in arsenite-treated HeLa cells. Biotinylated ribosomal DNA probes or a biotinylated poly(dT) probe were applied on thin sections and, after hybridization and washing, the hybrids were detected with an anti-biotin antibody coupled to 10 nm gold particles (Besse and Puvion-Dutilleul, 1996; Puvion-Dutilleul et al., 1994). The high specificity of this method is illustrated in supplementary material Fig. S3 by the cellular distribution of the 28S and 18S labelling. The background was evaluated by counting gold particles over the resin and was found to be less than 0.7±0.6 gold particles per μm^2 for all probes. To establish relative RNA contents, the density of gold particles was measured over the stress granules and the surrounding cytoplasm.

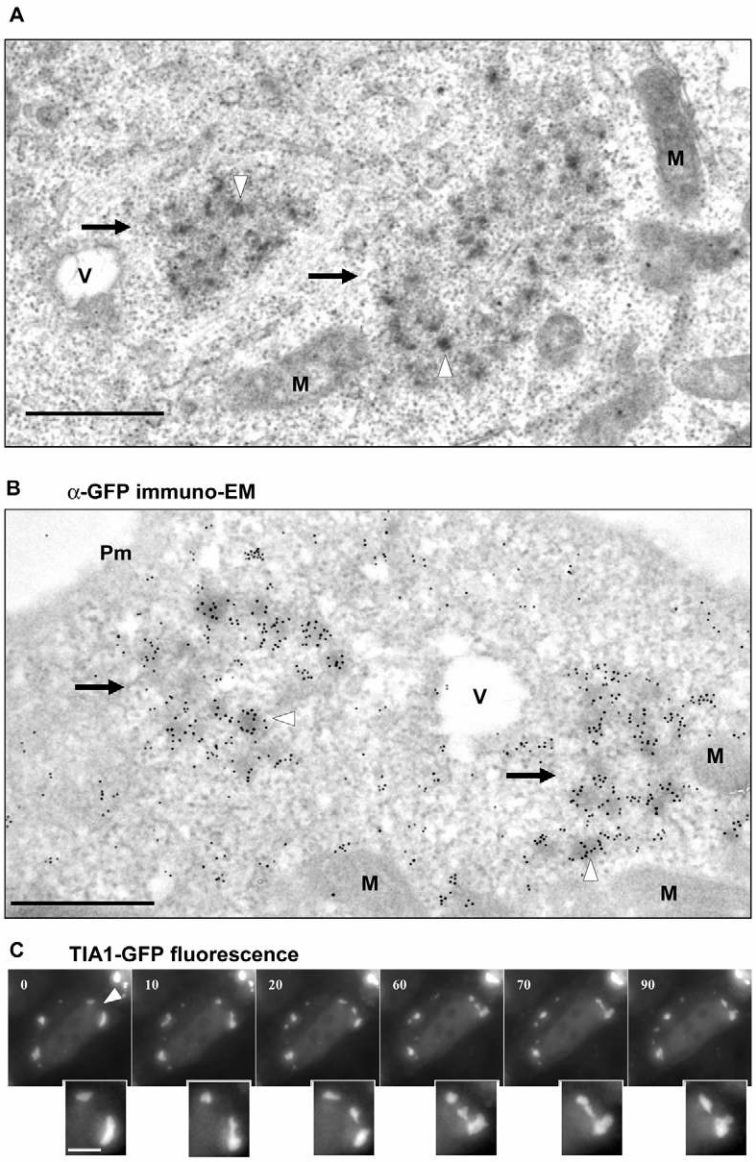

Fig. 4. Ultrastructure of TIA1-induced stress granules in HEK293 cells. (A) Thin section of a TIA1-GFP transfected HEK293 cell fixed in glutaraldehyde and embedded in Epon. Large cytoplasmic granules are conspicuous (black arrows). Note electron-dense fibrillar patches (white arrowheads) within these granules. V, vacuole; M, mitochondrion. Scale bar: 1 µm. (B) Detection of the TIA1-GFP fusion protein with an anti-GFP antibody in paraformaldehyde-fixed, Lowicryl-embedded HEK293 cells. Two cytoplasmic granules (black arrows) are highly labelled with gold particles particularly concentrated over the dense fibrillar patches (white arrowheads). The surrounding cytoplasm is also significantly labelled, indicating a high level of expression of the TIA1-GFP fusion protein in this particular cell. M, mitochondrion; V, vacuole; Pm, plasma membrane. Scale bar: 500 nm. (C) Continuous stress granule remodelling in live cells. TIA1-GFP transfected cells were observed by fluorescence microscopy for 90 minutes. The region indicated by an arrowhead is enlarged below, and shows a piece of stress granule transferred from one granule to another. Scale bars: 2 µm.

The 28S rRNA was depleted within stress granules (Fig. 5A), with a gold particle density only a third of the one measured in the surrounding cytoplasm, with 5.8±2 gold particles per μm^2 in stress granules versus 19.4±3 outside (n=12). By contrast, the 18S rRNA was enriched 1.8-fold (Fig. 5B), with 276±102 gold particles per μm^2 in stress granules, as compared with 154±34 in the surrounding cytoplasm (n=10). Similarly, polyadenylated mRNA was 4.4-fold enriched in stress granules (Fig. 5C), with a gold density of 38.0±9.8 per μm^2 as compared with 8.7±4.0 in the cytoplasm. Both 18S rRNA and mRNA were homogeneously distributed within the stress granules, indicating the absence of a radial distribution of the RNA. The sixfold enrichment of the 18S rRNA with respect to the 28S within stress granules indicates that monosomes are largely excluded from these structures.

Distinct ultrastructural features of stress granules and P-bodies

P-bodies have been defined by cryo-immunoelectron microscopy with an anti-GW182 antibody as non-membranous, roundish fibrillar bodies of a diameter of about 300 nm (Yang et al., 2004). However, no detailed ultrastructure in Epon-based, conventional electron microscopy has ever been reported, probably because of their paucity in thin sections. Arsenite treatment, aside from inducing stress granules, also increases the number of P-bodies (Serman et al., 2007; Wilczynska et al., 2005) (Fig. 6, left panels). Moreover, the induced stress granules and the numerous P-bodies are most often closely associated when simultaneously detected by immunofluorescence (Wilczynska et al., 2005) (Fig. 7A). We took advantage of this, to study the structure of P-bodies by conventional electron microscopy in arsenite-treated HeLa cells.

As a first step, we compared P-bodies in control and arsenite-treated HeLa cells by immunogold electron microscopy, using the endogenous Rck/p54 DEAD-box helicase as a marker. As shown in Fig. 6 (middle panels), Rck/p54 localization provides unambiguous detection of the P-bodies in Lowicryl embedded cells (similar results were obtained with an anti-Ge1 antibody, data not shown). In unstressed cells, P-bodies appear as densely labelled, roundish, electron dense bodies with a diameter of up to 300 nm (Fig. 6A), similar in size and shape with those detected by Yang et

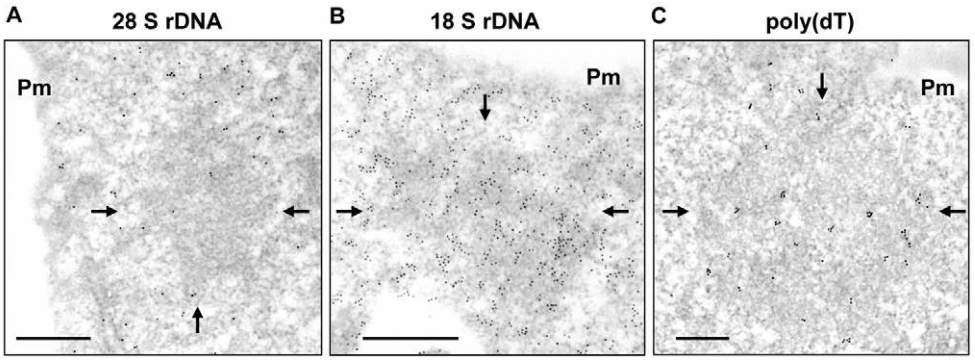

Fig. 5. RNA composition of arsenite-induced stress granules analysed by high resolution in situ hybridization in HeLa cells. HeLa cells were treated with arsenite for 30 minutes and processed for electron microscopy. Specific RNA species were hybridized with biotinylated DNA probes, as indicated, and revealed by immunodetection with an antibiotin antibody coupled to gold particles. As illustrated, the 28S rRNA is low in the stress granule indicated by black arrows (A), whereas the 18S rRNA (B) and the poly(A) RNA (C) are highly enriched. Notice that, despite high intensity of labelling, the extracellular resin is devoid of gold particles. Pm, plasma membrane. Scale bar: 500 nm.

al., using an anti-GW182 antibody (Yang et al., 2004). Moreover, at higher magnification (Fig. 6A, right panel), the gold particles could be seen to cluster on 10-15 nm strands (arrowheads). Following arsenite treatment, intense Rck/p54 labelling was found over P-bodies with the same ultrastructure (Fig. 6B). In particular, the fibrils were again apparent and highly decorated by the gold particles (Fig. 6B, right panel). Therefore, the short arsenite treatment enhances formation of typical P-bodies in HeLa cells.

Then, as suggested by immunofluorescence data (Fig. 7A), we found a number of thin-sections where P-bodies, labelled with anti-p54, were closely associated with a stress granule, identifiable by its characteristic finely granular structure (Fig. 7B). Close contact between the two structures was occasionally observed at this high resolution, but no intermingling. We then searched for stress-granule-associated P-bodies in Epon-embedded cells. We found large stress granules flanked by electron dense bodies, which by their size, shape and fibrillar structure were typical P-bodies (Fig. 7C,D). Epon-embedding amplified the differences between the fine structure of the two types of granules and made it possible to determine the detailed ultrastructure of the P-bodies. Aside from the 10-15 nm fibres described above, thinner contrasted fibbers of about 4 nm diameter that were up to 100 nm long were uncovered, as seen in the enlarged image in Fig. 7E. The exact composition of each type of fibrils remains to be determined.

Discussion

We have characterized, in detail, the ultrastructure of stress granules and associated P-bodies in the cytoplasm of mammalian cells using transmission electron microscopy. Their identity was confirmed by immunoelectron microscopy and by in situ hybridization on thin sections.

Stress granules are fibrillo-granular structures of a moderate electron density, with irregular outlines. Devoid of a membrane, they contain weakly aggregated granular particles resembling ribosomes within a loosely organized fibrillar cement. Their size, from one to several micrometers, and their texture are in full agreement with their appearance in fluorescence microscopy. Their poorly defined contour and their low level of compaction results in a non-uniform aspect previously observed for Dcp1 and Ge1, but not for eIF3, in immunofluorescence experiments, as well as for mRNA in FISH experiments (Mollet et al., 2008; Serman et al., 2007). In addition, stress granules assembled after heat shock or

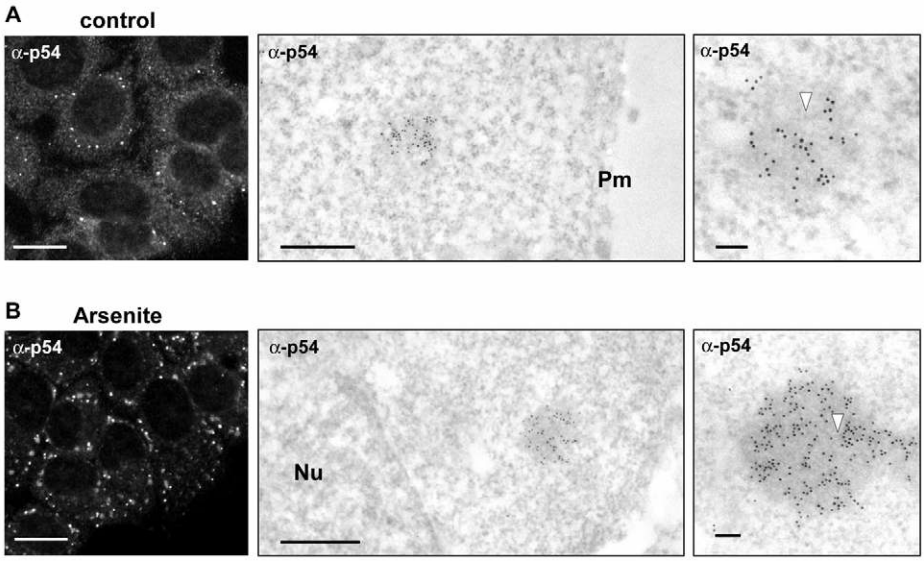

Fig. 6. Comparison of P-body ultrastructure in control and arsenite-treated HeLa cells. Control HeLa cells (A) and cells treated with arsenite for 30 minutes (B) were processed for immunofluorescence (left panels) or for immunoelectron (middle and right panels) microscopy with anti-p54 antibody. Endogenous Rck/p54 was identified in thin sections of Lowicryl embedded cells using a secondary antibody coupled to 10 nm gold particles. Pm, plasma membrane; Nu, nucleus. The induction of P-bodies by arsenite is visible in the left panel of B. In the middle panels, Rck/p54 can be seen to accumulate in roundish fibrillar structures with a diameter of 300-400 nm, consistent with the size of P-bodies detected by immunofluorescence. An enlarged view of a P-body is shown in the right panel, revealing tangentially cut 10-15 nm fibres indicated by arrowheads. Scale bars: 10 μm, 500 nm and 100 nm for left, middle and right panels, respectively.

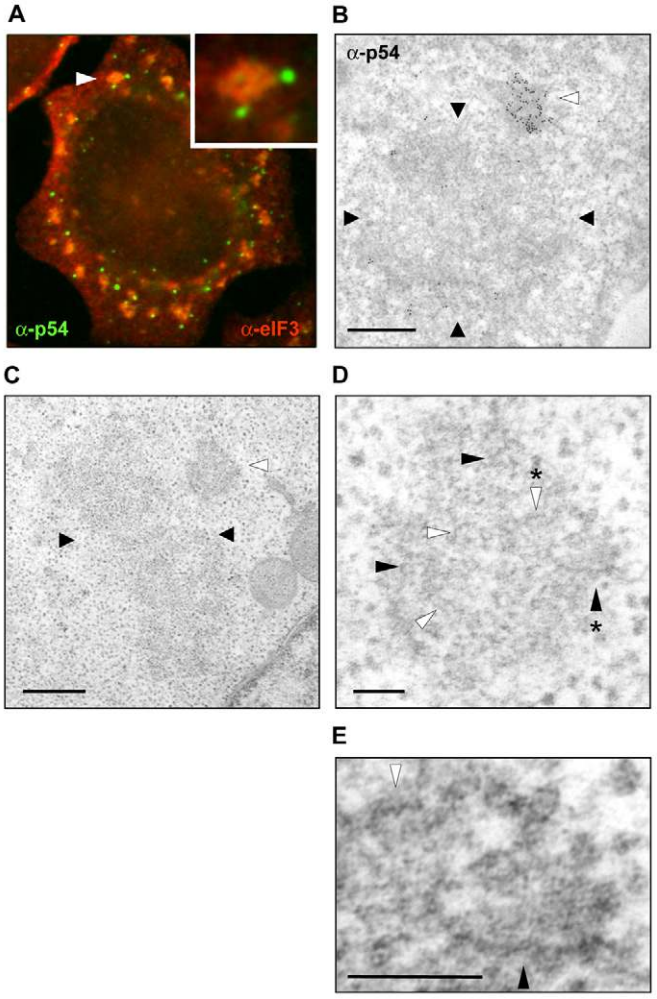

Fig. 7. Ultrastructural characterization of P-bodies in arsenite-treated HeLa cells. HeLa cells were treated with arsenite for 30 minutes and processed for immunofluorescence (A) or electron microscopy (B-E). (A) Stress granules and P-bodies were detected with anti-eIF3 (red) and anti-p54 (green) antibodies, respectively. P-bodies are frequently associated with stress granules, as indicate by the arrowhead and enlarged in the insert. (B) Endogenous Rck/p54 was detected in thin sections of Lowicryl embedded cells, as in Fig. 6. (C) Thin section of an Epon-embedded cell, as in Fig. 1. Both B and C show a P-body (white arrowhead) contacting a stress granule (black arrowhead). (D) Enlargement of a P-body embedded in Epon reveals 10-15 nm (black arrowheads) and 4 nm (white arrowheads) fibres. The region encompassing the 10-15 nm and 4 nm fibres marked by a star is further enlarged in E. Scale bars: 500 nm (B,C); 100 nm (D,E).

following TIA1 overexpression include characteristic dense fibrillar patches. Finally, stress granules often include small regions of cytoplasm, which could be trapped during stress granule assembly (Mollet et al., 2008) or appear in the course of their continuous remodelling, as observed in live cells. In the current models of stress granule assembly, mRNPs aggregate locally by virtue of the self-aggregating properties of RNA-binding proteins, such as TIA1. Their continuous remodelling in live cells and their loose ultrastructure seen in electron microscopy indicate that aggregation is weak or can be easily broken. This suggests that stress granules will be difficult to isolate by fractionation for detailed biochemical analysis.

Our observations contrast with a previous cryoelectron microscopy study of stress granules induced by HA-tagged TIA1 overexpression in COS7 cells. Small globular aggregates of 100-200 nm diameter ringed by a corona of particles that resemble ribosomes have been described (Gilks et al., 2004). Because stress granules are about ten times larger when examined in fluorescence microscopy, the authors speculated that these globular aggregates were subcomponents of the stress granules. Similar small aggregates were also observed in pyramidal neurons of normal brain, using transmission electron microscopy (Kayali et al., 2005). Their number increased following ischemia-reperfusion of the brain, but they did not coalesce to form larger granules. As we did not observe such structure, either in arsenite-treated or heat shocked HeLa or HEK293 cells, or in HEK293 cells transfected with GFP-tagged TIA1 or CPEB1, despite the induction of typical stress granules, we suggest that these 100 nm globular granules are unrelated to stress granule.

Originally, cytoplasmic stress granules were described in tomato cell lines submitted to heat shock. Masses of regularly ordered 30-40 nm particles were found as a result of heat shock and of the ensuing translational arrest (Nover et al., 1983). This was confirmed in tobacco cells, using electron microscopy with procedures similar to ours (Miroshnichenko et al., 2005). No such regularly arranged arrays of particles were ever seen in our study. However, a recent publication based on wide-field fluorescence microscopy clearly distinguished two types of cytoplasmic stress granules in plants: heat stress granules (HSG), which are induced by prolonged exposure to heat, require the accumulation of heat shock proteins, and contain little mRNA, and mammalian-like stress granules (SG) which are induced by a brief heat shock independently of heat shock proteins and are enriched in mRNAs (Weber et al., 2008). The original description of cytoplasmic stress granules in plants, as seen by electron microscopy, corresponds to that of HSGs. Thus, our study is the first ultrastructural characterization of SG in eukaryotic cells.

The detailed mechanism by which translational repressors such as TIA1 or CPEB1 can induce stress granules is currently unknown, although it seems to require a certain threshold of expression. TIA1 is an RNA-binding protein involved in post-transcriptional regulations, at the level of both splicing and translation (Lopez de Silanes et al., 2005; McAlinden et al., 2007). In the context of translation, a systematic analysis of TIA1-bound mRNAs indicated that they contain a specific U-rich element in their 3′ untranslated region. These mRNAs correspond to 3% of the Unigene database, indicating that TIA1 is a specific translational regulator (Lopez de Silanes et al., 2005). At first sight, TIA1-induced stress granules could specifically contain these TIA1 target mRNAs. Electron microscopy makes it possible to distinguish free ribosomes from polysomes, the latter forming typical rosette patterns, which are probably mRNP with a closed loop configuration. Interestingly, the cytoplasm of the cells containing TIA1-induced stress granules is devoid of such rosettes, to the same extent as arsenite-treated and heat-shocked cells. This indicates a general, rather than specific, translational arrest in these cells. A high level of TIA1 expression therefore disturbs the general translation machinery. Similarly, CPEB1 specifically controls the translation of CPE-containing mRNAs. Nonetheless, CPEB1-induced stress granules are only observed in non-translating cells.

The rRNA and mRNA content of stress granules was analysed by in situ hybridization. It confirmed the enrichment of 18S rRNA and mRNA, and the exclusion of 28S rRNA, in agreement with previous immunofluorescence experiments using antibodies against

various ribosomal proteins, and FISH with an oligo(dT) probe (Kedersha et al., 2002). In addition, in situ hybridization on thin sections offered the opportunity to quantify the relative abundance of rRNA and mRNA with respect to the surrounding cytoplasm. Messenger RNA and 18S rRNA were, respectively, 4.4- and 1.8-fold more concentrated in the stress granules whereas 28S rRNA was 3.3-fold more concentrated in the cytosol. Thus, stress granules accumulate mRNAs, potentially associated with the small ribosomal subunit, but not with ribosomes. However, taking into account the volume of cytoplasm occupied by the stress granules, it also indicates that the majority of the arrested mRNAs is not confined to the stress granules. After 30 minutes of arsenite treatment, translation is fully arrested and stress granules are present in all cells. Yet, stress granules occupy only about 3% of the volume of the cytoplasm as estimated by confocal microscopy analysis (data not shown). Accordingly, they are visible in only 1/10 of the cells in the thin sections of 70 nm used for electron microscopy. Taking into account the measured 4.4-fold enrichment in poly(A)+ RNA, at a given time point, only about 15% of the cellular mRNAs are in stress granules. This confirms our previous estimate that was based on the measurement of an MS2-tagged reporter mRNA by fluorescence microscopy (Mollet et al., 2008). It would now be interesting to determine whether the stress granules selectively accumulate all the mRNAs that are bound to the small ribosomal subunit. This could be the case if stress granules are involved in translation initiation during stress, as recently proposed by Buchan and collegues in yeast (Buchan et al., 2008). Although consistent with such a hypothesis, our in situ hybridization data, however, cannot distinguish free and associated 18S and mRNA molecules.

Our data on P-body ultrastructure is in full agreement with a previous study using immunoelectron microscopy, which showed that P-bodies have a fibrillar ultrastructure (Yang et al., 2004). The Rck/p54 RNA helicase, which is highly concentrated in P-bodies, is localized on fibrils of 10-15 nm diameter in both untreated and arsenite-treated cells, as was observed for GW182 (Yang et al., 2004). We believe that these fibres are the same as the 8-10 nm strands described previously (Yang et al., 2004), considering that, in both studies, the strands are slightly larger than the 10 nm gold particles used for the labelling. The exact thickness of the strands can be affected by the different protocols used in the two studies: cryo-electron microscopy with anti-GW182 antibody (Yang et al., 2004) versus Lowicryl thin sections with anti-p54 antibody (our study). Further analysis at higher resolution in Epon resin revealed additional fibres of about 4 nm diameter, which are somewhat reminiscent of perichromatin fibrils, the mRNPs corresponding to nascent nuclear transcripts, particularly in their decondensed state (Puvion-Dutilleul and Puvion, 1980). It is noteworthy that P-bodies do not contain granular particles. By comparison, nuclear mRNPs are fibrillar during transcription and release, and then become roundish, granular particles up to 35-50 nm in diameter, probably by twisting of the 4 nm fibrils (Fakan and Puvion, 1980).

P-bodies do not rearrange as actively as stress granules, fusions and fissions being seen only occasionally in live cells (Kedersha et al., 2005) (and data not shown). Accordingly, their structure is more compact. Overall, beyond the difference of shape and size, P-bodies and stress granules can be recognized by their respective ultrastructure, the former being compact and fibrillar and the latter loose and fibrillo-granular. Although stress granules have been shown to assemble on pre-existing P-bodies in mammalian cells and in yeast, their distinct ultrastructure suggests that the former are not a simple extension of the latter. Stress granules and P-bodies are frequently seen adjacent to one another by fluorescence microscopy. By electron microscopy we show that these contacts are intimate. Although such proximity supports the possibility that proteins and/or RNA can transfer from one structure to the other, experimental evidence for this traffic is lacking. When studying proteins shared by the two compartments, we found previously that proteins present in the stress granules originated not from the neighbouring P-bodies, but from the cytosol (Mollet et al., 2008). With this study, we now show that, if such an exchange exists, it is not attested by any interpenetration of the two compartments, which remain always well individualized.

Materials and Methods

Cell culture

Epithelioid carcinoma HeLa and human embryonic kidney HEK293 cells were routinely maintained in DMEM supplemented with 10% fetal calf serum. For stress induction, cells were treated with 0.5 mM arsenite (Sigma-Aldrich, France) for 30 minutes or heated at 42°C for 30 minutes.

HEK293 cells were chosen for their high transfection efficiency (close to 90% in our conditions). Transient transfections were performed with 10 μg plasmid DNA per 10 cm diameter dish using a standard calcium phosphate procedure. GFP-TIA1 was a kind gift from Veronique Kruys (Université libre de Bruxelles, Brussels, Belgium) (Zhang et al., 2005).

Fluorescence microscopy

For immunofluorescence, cells were grown on glass coverslips and fixed in –20°C methanol for 3 minutes. Cells were incubated with the primary antibody for 1hour, rinsed with phosphate-buffered saline (PBS), incubated with the secondary antibody for 30 minutes and rinsed with PBS; all steps were performed at room temperature. Slides were mounted in Citifluor (Citifluor, UK). Goat polyclonal anti-eIF3 antibody was a kind gift from John Hershey (University of California, Davis, CA) and rabbit polyclonal anti-p54 was purchased from Bethyl Laboratories (Montgomery, TX). Secondary antibodies conjugated to Cy3 and Cy2 were purchased from Jackson Immunoresearch (Interchim, Montluçon, France).

Standard microscopy was performed on a Leica DMR microscope (Leica, Heidelberg, Germany) using a 63× 1.32 oil immersion objective. Photographs were taken using a Micromax CCD camera (Princeton Instruments, Princeton, NJ). For videomicroscopy, cells were grown on glass coverslips and mounted in a POC chamber system (Helmut Saur, Reutlingen, Germany) with 2 ml culture medium maintained at 37°C and 5% CO_2. Cells were observed on a Zeiss Axiovert inverted microscope (Carl Zeiss SAS, Le Pecq, France) equipped with a DG4 Lambda switcher (Sutter Instrument, Novato, CA) and driven by Metamorph software (Universal Imaging, Downingtown, PA). Timed series were acquired using a 63× 1.32 oil immersion objective.

Biotinylated probes for high resolution in situ hybridization

A synthetic poly(dT) with an average length of 174 nucleotides (nt) (Pharmacia) was biotinylated with biotin-16-dUTP (Roche Diagnostics, Mannheim) in the presence of terminal deoxynucleotidyl transferase (BioLabs). Reaction time was 2 hours at 37°C in a 20 μl final volume with 2.7 μg of polynucleotide, 25 IU terminal deoxynucleotidyl transferase and 1.5 mM $CoCl_2$. The reaction was stopped by the addition of 200 μl 12.5 mM EDTA, pH 8.0. Following addition of 100 μl of 1 M sodium acetate, pH 5.2 and 10 μg of carrier tRNA, the biotinylated poly(dT) was ethanol precipitated. After one additional cycle of dissolution and ethanol precipitation, the probe was dissolved in water (50 μg/ml) and frozen at –20°C until use.

rDNA probes for the 18S or the 28S ribosomal RNAs were made by biotinylation of DNA fragments amplified by PCR from cosmid 11.36, which contains a complete copy of the human rDNA repeat (kindly provided by Jérôme Cavaillé, LMBE, Toulouse, France) (Renalier et al., 1989). For the 18S rDNA probe, a 1383 bp fragment was amplified by PCR with primers corresponding to nt 346-374 (5′-TCTGCCCT-TCAACTATTTCGATGG-3′) and 1729-1708 (5′-CCATCCAATCGGTAGTAGC-GAC-3′) of the human 18S ribosomal RNA (NR_003286.1). For the 28S rDNA probe, DNA fragments of 768 bp and 1105 bp were separately amplified with primers corresponding to nt 1235-1254 (5′-ACGTCGGCTACCCACCCGAC-3′) and nt 2003-1987 (5′-CCGACGCTCCAGCGCCATC-3′) or nt 3528-3547 (5′-TAGCAGCCG-ACTTAGAACTG-3′) and nt 4633-4614 (5′-ATTCTGACTTAGAGGCGTTC-3′), respectively, of the human 28S ribosomal RNA (NR_003287.1). Amplification products were purified on microcon YM-100 (Millipore) and biotinylated using a nick-translation kit from Roche Diagnostics. One μg of the 18S amplified DNA fragment or 0.5 μg of the two 28S amplicons were used as substrates in a 20 μl reaction carried out in the presence of dATP, dCTP and dGTP, 0.02 mM each, and 0.05 mM biotin-16-dUTP for 3 hours at 15°C. The reaction product was then frozen at –20°C until use.

Fixation and embedding for electron microscopy

For Epon embedding, cell cultures were fixed for 1 hour at 4°C in 1.6% glutaraldehyde (Taab Laboratory Equipment, Reading, UK) in 0.1 M phosphate buffer, pH 7.3. During fixation, cells were scraped from the plastic substratum and centrifuged. Cell pellets were dehydrated in increasing concentrations of ethanol and embedded in Epon. Polymerization was carried out for 48 hours at 64°C. Ultrathin sections were collected on Formvar-carbon-coated copper grids (200 mesh).

For embedding in Lowicryl K4M (Chemische Werke Lowi, Waldkraiburg, Germany), cell cultures were fixed either in 4% formaldehyde (Merck, Darmstadt, Germany) or in 1.6% glutaraldehyde at 4°C and dehydrated in increasing concentrations of methanol. Embedding was carried out at low temperature according to Roth (Roth, 1989). Polymerization was at –30°C for 5 days under long wavelength UV light. Ultrathin sections of Lowicryl-embedded material were collected on Formvar-carbon-coated gold grids (200 mesh) and stored until use. The sections were analysed with a FEI Tecnai Spirit transmission electron microscope, and digital images were taken with a SIS MegaviewIII CCD camera.

Localization of proteins by immunoelectron microscopy

For immunolocalization of proteins, glutaraldehyde-fixed Lowicryl-embedded thin sections were first reacted with the primary antibody diluted in PBS (anti-p54) or in PBS with 1% BSA and 0.1% Triton X-100 (anti-GFP) for 1 hour at room temperature. After washing in PBS, grids were incubated for 30 minutes at room temperature with the goat anti-rabbit secondary antibody coupled to 10 nm gold particles, diluted in PBS. Following final washing in PBS, grids were rapidly rinsed in a jet of distilled water, air-dried, and counterstained with 4% uranyl acetate. Rabbit polyclonal anti-GFP (Abcam) and anti-p54 (Bethyl Laboratories, Montgomery, TX) antibodies were used at a dilution of 1/100 and goat anti-rabbit secondary antibody coupled to 10 nm gold particles (BBInternational) at a dilution of 1/25.

In situ hybridization at the ultrastructural level.

Hybridization was performed as previously described for poly(dT) and ribosomal DNA probes (Puvion-Dutilleul et al., 1991; Visa et al., 1993). The hybridization solution contained 50% deionized formamide, 10% dextran sulphate, 2× SSC and either 35 μg/ml tRNA and 10 μg/ml biotinylated poly(dT) for poly(A)$^+$ mRNA detection or 400 μg/ml of competitor *E. coli* DNA, and 8 μg/ml of biotinylated double-stranded amplified rDNA for ribosomal RNA detection. In this latter case, the hybridization solution was heat-treated for 4 minutes just before use, in order to denature the double-stranded DNA probes. The grids bearing sections of formaldehyde-fixed cells were placed in contact with the hybridization solution and incubated for 90 minutes at 37°C for poly(A)$^+$ mRNA detection and 3 hours at 65°C for rRNA detection. Biotin-containing hybrids were revealed directly by using goat anti-biotin antibody conjugated to 10 nm gold particles (BB International), diluted 1/25 in PBS, for 30 minutes at room temperature. Subsequently, grids were washed and stained with 4% uranyl acetate prior to observation. The specificity of the hybridization signals was assessed by negative results when sections were pretreated with 1 mg/ml RNase A (BDH Biochemical, UK) for 1 hour at 37°C in 10 mM Tris-HCl buffer, pH 7.3.

Quantifications

For each sample, 10-15 thin sections were analysed at a final magnification of 60,000× to 80,000×. The micrographs were selected for stress granules of 0.6 μm^2 or more, and images were taken of large cytoplasmic and extracellular (pure resin) areas, for comparison of gold densities and for background evaluation, respectively. Surface areas were determined with analySIS, the software attached to the SIS Megaview camera, and gold particles were counted by eye. Gold particle density and standard deviation were calculated using Microsoft Excel.

We thank Jérôme Cavaillé for providing a human rDNA repeat. S.M. was supported by a fellowship from the Ministère de l'Enseignement Supérieur. This work was supported by the Centre National de la Recherche Scientifique, the Association pour la Recherche contre le Cancer, and the Agence Nationale pour la Recherche.

References

Anderson, P. and Kedersha, N. (2008). Stress granules: the Tao of RNA triage. *Trends Biochem. Sci.* **33**, 141-150.

Besse, S. and Puvion-Dutilleul, F. (1996). Intranuclear retention of ribosomal RNAs in response to herpes simplex virus type 1 infection. *J. Cell Sci.* **109**, 119-129.

Bhattacharyya, S. N., Habermacher, R., Martine, U., Closs, E. I. and Filipowicz, W. (2006). Relief of microRNA-mediated translational repression in human cells subjected to stress. *Cell* **125**, 1111-1124.

Brengues, M., Teixeira, D. and Parker, R. (2005). Movement of eukaryotic mRNAs between polysomes and cytoplasmic processing bodies. *Science* **310**, 486-489.

Buchan, J. R., Muhlrad, D. and Parker, R. (2008). P bodies promote stress granule assembly in Saccharomyces cerevisiae. *J. Cell Biol.* **183**, 441-455.

Cougot, N., Babajko, S. and Seraphin, B. (2004). Cytoplasmic foci are sites of mRNA decay in human cells. *J. Cell Biol.* **165**, 31-40.

Eulalio, A., Behm-Ansmant, I. and Izaurralde, E. (2007). P bodies: at the crossroads of post-transcriptional pathways. *Nat. Rev. Mol. Cell Biol.* **8**, 9-22.

Fakan, S. and Puvion, E. (1980). The ultrastructural visualization of nucleolar and extranucleolar RNA synthesis and distribution. *Int. Rev. Cytol.* **65**, 255-299.

Gilks, N., Kedersha, N., Ayodele, M., Shen, L., Stoecklin, G., Dember, L. M. and Anderson, P. (2004). Stress granule assembly is mediated by prion-like aggregation of TIA-1. *Mol. Biol. Cell* **15**, 5383-5398.

Hoyle, N. P., Castelli, L. M., Campbell, S. G., Holmes, L. E. and Ashe, M. P. (2007). Stress-dependent relocalization of translationally primed mRNPs to cytoplasmic granules that are kinetically and spatially distinct from P-bodies. *J. Cell Biol.* **179**, 65-74.

Kayali, F., Montie, H. L., Rafols, J. A. and DeGracia, D. J. (2005). Prolonged translation arrest in reperfused hippocampal cornu Ammonis 1 is mediated by stress granules. *Neuroscience* **134**, 1223-1245.

Kedersha, N., Chen, S., Gilks, N., Li, W., Miller, I. J., Stahl, J. and Anderson, P. (2002). Evidence that ternary complex (eIF2-GTP-tRNA(i)(Met))-deficient preinitiation complexes are core constituents of mammalian stress granules. *Mol. Biol. Cell* **13**, 195-210.

Kedersha, N., Stoecklin, G., Ayodele, M., Yacono, P., Lykke-Andersen, J., Fritzler, M. J., Scheuner, D., Kaufman, R. J., Golan, D. E. and Anderson, P. (2005). Stress granules and processing bodies are dynamically linked sites of mRNP remodeling. *J. Cell Biol.* **169**, 871-884.

Lopez de Silanes, I., Galban, S., Martindale, J. L., Yang, X., Mazan-Mamczarz, K., Indig, F. E., Falco, G., Zhan, M. and Gorospe, M. (2005). Identification and functional outcome of mRNAs associated with RNA-binding protein TIA-1. *Mol. Cell. Biol.* **25**, 9520-9531.

Mazroui, R., Sukarieh, R., Bordeleau, M. E., Kaufman, R. J., Northcote, P., Tanaka, J., Gallouzi, I. and Pelletier, J. (2006). Inhibition of ribosome recruitment induces stress granule formation independently of eukaryotic initiation factor 2alpha phosphorylation. *Mol. Biol. Cell* **17**, 4212-4219.

McAlinden, A., Liang, L., Mukudai, Y., Imamura, T. and Sandell, L. J. (2007). Nuclear protein TIA-1 regulates COL2A1 alternative splicing and interacts with precursor mRNA and genomic DNA. *J. Biol. Chem.* **282**, 24444-24454.

McInerney, G. M., Kedersha, N. L., Kaufman, R. J., Anderson, P. and Liljestrom, P. (2005). Importance of eIF2alpha phosphorylation and stress granule assembly in alphavirus translation regulation. *Mol. Biol. Cell* **16**, 3753-3763.

Miroshnichenko, S., Tripp, J., Nieden, U., Neumann, D., Conrad, U. and Manteuffel, R. (2005). Immunomodulation of function of small heat shock proteins prevents their assembly into heat stress granules and results in cell death at sublethal temperatures. *Plant J.* **41**, 269-281.

Mollet, S., Cougot, N., Wilczynska, A., Dautry, F., Kress, M., Bertrand, E. and Weil, D. (2008). Translationally repressed mRNA transiently cycles through stress granules during stress. *Mol. Biol. Cell* **19**, 4469-4479.

Nover, L., Scharf, K. D. and Neumann, D. (1983). Formation of cytoplasmic heat shock granules in tomato cell cultures and leaves. *Mol. Cell. Biol.* **3**, 1648-1655.

Puvion-Dutilleul, F. and Puvion, E. (1980). New aspects of intranuclear structures following partial decondensation of chromatin: a cytochemical and high-resolution autoradiographical study. *J. Cell Sci.* **42**, 305-321.

Puvion-Dutilleul, F., Bachellerie, J. P. and Puvion, E. (1991). Nucleolar organization of HeLa cells as studied by in situ hybridization. *Chromosoma* **100**, 395-409.

Puvion-Dutilleul, F., Bachellerie, J. P., Visa, N. and Puvion, E. (1994). Rearrangements of intranuclear structures involved in RNA processing in response to adenovirus infection. *J. Cell Sci.* **107**, 1457-1468.

Renalier, M. H., Mazan, S., Joseph, N., Michot, B. and Bachellerie, J. P. (1989). Structure of the 5′-external transcribed spacer of the human ribosomal RNA gene. *FEBS Lett.* **249**, 279-284.

Roth, J. (1989). Postembedding labeling on Lowicryl K4M tissue sections: detection and modification of cellular components. *Methods Cell Biol.* **31**, 5135-5151.

Serman, A., Le Roy, F., Aigueperse, C., Kress, M., Dautry, F. and Weil, D. (2007). GW body disassembly triggered by siRNAs independently of their silencing activity. *Nucleic Acids Res.* **35**, 4715-4727.

Teixeira, D., Sheth, U., Valencia-Sanchez, M. A., Brengues, M. and Parker, R. (2005). Processing bodies require RNA for assembly and contain nontranslating mRNAs. *RNA* **11**, 371-382.

Visa, N., Puvion-Dutilleul, F., Bachellerie, J. P. and Puvion, E. (1993). Intranuclear distribution of U1 and U2 snRNAs visualized by high resolution in situ hybridization: revelation of a novel compartment containing U1 but not U2 snRNA in HeLa cells. *Eur. J. Cell Biol.* **60**, 308-321.

Warner, J. R., Rich, A. and Hall, C. E. (1962). Electron microscope studies of ribosomal clusters synthesizing hemoglobin. *Science* **138**, 1399-1403.

Weber, C., Nover, L. and Fauth, M. (2008). Plant stress granules and mRNA processing bodies are distinct from heat stress granules. *Plant J.* **56**, 517-530.

Wilczynska, A., Aigueperse, C., Kress, M., Dautry, F. and Weil, D. (2005). The translational regulator CPEB1 provides a link between dcp1 bodies and stress granules. *J. Cell Sci.* **118**, 981-992.

Yang, W. H. and Bloch, D. B. (2007). Probing the mRNA processing body using protein macroarrays and "autoantigenomics". *RNA* **13**, 704-712.

Yang, W. H., Yu, J. H., Gulick, T., Bloch, K. D. and Bloch, D. B. (2006). RNA-associated protein 55 (RAP55) localizes to mRNA processing bodies and stress granules. *RNA* **12**, 547-554.

Yang, Z., Jakymiw, A., Wood, M. R., Eystathioy, T., Rubin, R. L., Fritzler, M. J. and Chan, E. K. (2004). GW182 is critical for the stability of GW bodies expressed during the cell cycle and cell proliferation. *J. Cell Sci.* **117**, 5567-5578.

Zhang, T., Delestienne, N., Huez, G., Kruys, V. and Gueydan, C. (2005). Identification of the sequence determinants mediating the nucleo-cytoplasmic shuttling of TIAR and TIA-1 RNA-binding proteins. *J. Cell Sci.* **118**, 5453-5463.